Guiding of Rydberg atoms in a high-gradient magnetic guide

M. Traxler,[1] R. E. Sapiro,[1] C. Hempel,[2] K. Lundquist,[1] E. P. Power,[1] and G. Raithel[1]
[1]*Department of Physics, University of Michigan, Ann Arbor, Michigan 48109, USA*
[2]*Institute for Quantum Optics and Quantum Information, Innsbruck A-6020, Austria*
(Received 3 February 2012; revised manuscript received 25 June 2012; published 20 August 2012)

We study the guiding of ^{87}Rb $59D_{5/2}$ Rydberg atoms in a linear, high-gradient, two-wire magnetic guide. Time-delayed microwave ionization and ion detection are used to probe the Rydberg atom motion. We observe guiding of Rydberg atoms over a period of 5 ms following excitation. The decay time of the guided-atom signal is about five times that of the initial state. We attribute the lifetime increase to an initial phase of l-changing collisions and thermally induced Rydberg-Rydberg transitions. Detailed simulations of Rydberg-atom guiding reproduce most experimental observations and offer insight into the internal-state evolution.

DOI: 10.1103/PhysRevA.86.023414 PACS number(s): 37.10.Gh

I. INTRODUCTION

There has been a recent surge of interest in cold Rydberg atoms in a linear trapping geometry. Such systems present the possibility of creating one-dimensional spin chains by exciting atoms into high-lying Rydberg levels, which interact strongly due to their large dipole moments [1–3]. Rydberg crystals, which have been proposed in a frozen atomic gas using the Rydberg excitation blockade effect, may be an interesting application within a linear structure [4]. Entangled Rydberg atoms prepared in a linear guiding geometry could act as a shuttle for quantum information [5,6]. A one-dimensional trap or guide for Rydberg atoms could be used to further these types of research. Cold Rydberg atoms have been experimentally trapped using magnetic [7], electrostatic [8], and light fields [9]. Conservative trapping of Rydberg atoms in magnetic atom guides has been theoretically investigated in Refs. [10–12]. Theoretical calculations also indicate the possibility of stationary Rydberg atoms confined in magnetic traps and magnetoelectric traps [13–15]. These systems would allow one to study Rydberg gases in a one-dimensional geometry. The Rydberg-Rydberg interaction properties in such a system have been studied theoretically in Ref. [16].

Waveguides built into chips are attractive setups for the linear guiding of atoms, and much experimental work [17–19] has advanced this type of research. With the capability of high magnetic gradients at low currents, such systems can be significantly smaller than macroscopic versions of magnetic guides. However, chip-based waveguides come at the price of having larger stray electric fields [20]. Though it takes much more physical space than an atom chip, we find that our large magnetic guide is a good environment in which to study the guiding of Rydberg atoms in a linear magnetic guide.

II. EXPERIMENTAL SETUP

The magnetic guide utilized in this work is formed by two parallel wires with an average center-to-center separation of 4.5 mm that are ∼1.5 m long and carry parallel currents of 200 A. This structure creates a single magnetic field minimum along the symmetry line between the two wires, which provides a guiding channel for low magnetic field seeking atoms. The transverse magnetic field gradient is ∼1.5 kG/cm. This is quite high for macroscopic nonsuperconducting traps and similar to the gradient assumed in Ref. [13]. The guiding potential is $\mu_B g_j m_j |B|$, where μ_B is the Bohr magneton, g_j is the Landé g factor, m_j is the magnetic quantum number, and B is the magnetic field. A bias field of several gauss pointing along the guide prevents losses from spin flips. The atom guide confines a beam of ^{87}Rb atoms prepared in the $|F = 1, m_F = -1\rangle$ level of the $5S_{1/2}$ ground state; the guiding potential for this state is $\frac{1}{2}\mu_B|B|$. The atomic beam diameter is ≈200 μm and the flux is $\sim 2 \times 10^7$ s^{-1}. The forward velocity of the guided atoms is adjusted to ≈1 m/s. The ground-state atoms have transverse and longitudinal temperatures of $T_{x,y} \approx 400$ μK and $T_z \approx 1$ mK, respectively. The temperatures were derived from measurements of the atom distribution within the magnetic guide and from time-of-flight measurements [21,22]. A fraction of the ground-state atom flow is excited into Rydberg levels, and we examine the guiding of these Rydberg atoms. This low-field, high-gradient, room-temperature setup differs significantly from previous high magnetic field superconducting traps for Rydberg atoms [7].

The excitation and detection region for Rydberg atoms is located 85 cm down the guide, illustrated in Fig. 1. The length of the guide segment that is relevant to the Rydberg atom guiding work described in this paper, highlighted in Fig. 1, is about 1 cm long. We use a three-step Rydberg atom excitation process. A pulsed 780 nm beam (with a duration of 10 μs) pumps the atoms from $5S_{1/2}$ $|F = 1, m_F = -1\rangle$ to $F = 2$. A second pulsed 780 nm beam (with a duration of 5 μs) subsequently drives the atoms on the cycling transition into $5P_{3/2}$ $F' = 3$. The atoms are excited from the $5P_{3/2}$ level to the $59D_{5/2}$ Rydberg level with a tunable, continuous 480 nm beam. The electric field in the guiding region is zeroed by adjusting the potential of the electrode and the potential difference between the guide wires identified in Fig. 1.

The Rydberg atoms are probed by ionization with a microwave pulse of 20 μs duration and 18.5 GHz frequency. The microwave pulse is applied at a variable delay time t_d and ionizes more than 90% of the Rydberg atoms. After ionization the free charges are decoupled from the microwaves; i.e., the ions are no longer affected by the microwave field due to their vanishing ponderomotive energy and quiver amplitudes in the microwave field. With the electric field zeroed, about half of the ions drift downward and are lost. The other half

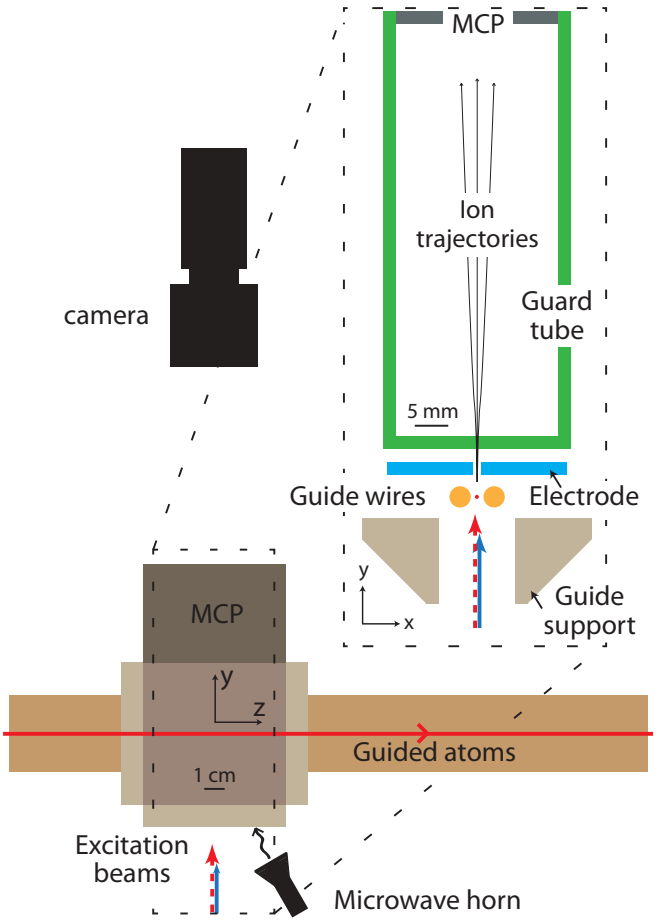

FIG. 1. (Color online) Schematic of the excitation and detection region in the two-wire magnetic guide. The guided atoms (small red dot) travel between the guide wires, where they are excited into Rydberg levels with two lower (780 nm, dashed red arrow) and one upper (480 nm, solid blue arrow) transition beams. The Rydberg atoms are detected by microwave ionization. With the guide support grounded and the guard tube at −1.4 kV, ions are directed upward to a microchannel plate (MCP), where counts are recorded with both spatial and temporal resolution.

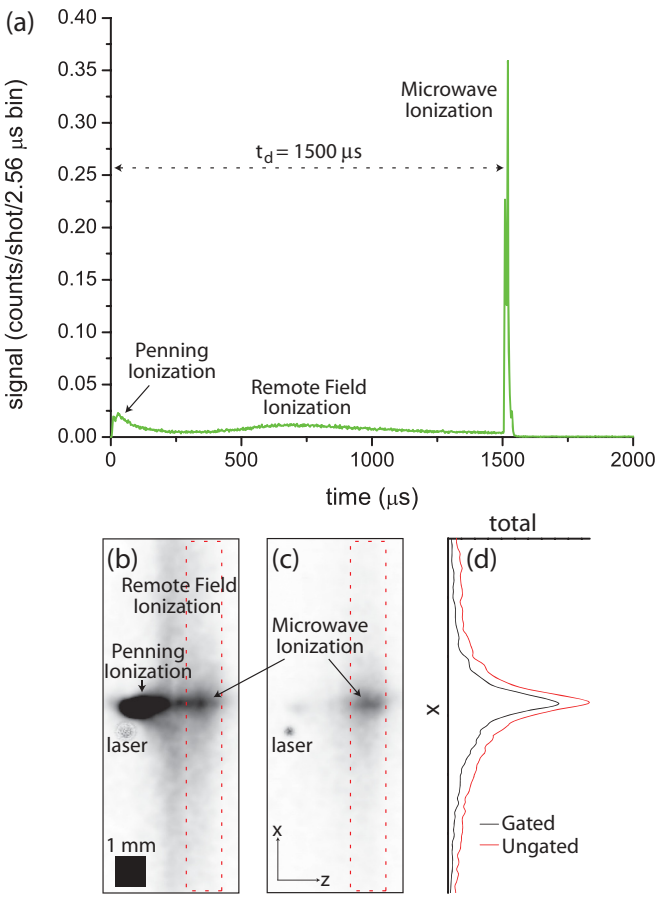

FIG. 2. (Color online) (a) MS trace, at $t_d = 1.5$ ms. MCP image with a delay time of $t_d = 1.5$ ms, with (b) camera on throughout the experimental cycle and (c) camera gated over the microwave ionization signal. The black square indicates 1 mm^2 in the image plane. The images exhibit a remnant of laser light penetrating through the MCP and phosphor screen. (d) Profiles of each from the regions indicated by the dashed boxes.

drift upward into the electric field generated by the guard tube, held at −1.4 kV, which accelerates them to a microchannel plate (MCP). We estimate the MCP detection efficiency at 1.4 keV ion energy to be about 30% [23]. Hence the overall Rydberg atom detection efficiency is estimated to be ∼15%. Each detected ion produces a countable pulse and a blip on a phosphor screen behind the MCP. We note that ion detection is necessary instead of electron detection because the magnetic fields from the guide wires remain on throughout the entire experiment [24].

The temporal distribution of the MCP pulses is recorded using a multichannel scaler (MS). The MS traces presented in this paper are averages over up to 50 000 experimental cycles. The spatial distribution is recorded with a CCD camera, which images the blips on the MCP phosphor screen. All images presented are an average of 30 000 images with a background (30 000 images without an atomic beam) subtracted. A sample of both types of data is shown in Fig. 2.

III. EXPERIMENTAL RESULTS

To show guiding of Rydberg atoms, we ionize the Rydberg atoms in our guide at delay times that range from 5 μs to 5 ms. We use the data for $t_d = 1.5$ ms, shown in Fig. 2, to provide an overview of several important observations of this experiment, which will be discussed in more detail throughout the remainder of the paper. The microwave ionization signal occurs in the time traces at time t_d. The corresponding counts from the microwave ionization are labeled in the images. Before the microwaves are applied, we observe Penning ionization and remote field ionization. Both of these signals arise from the geometry of our setup and do not play a large role in the analysis of the Rydberg guiding, though are relevant to the overall evolution of the Rydberg atom sample. We use the microwave ionization signals in both the time traces and the images to show that the Rydberg atoms are guided. We also determine the initial Rydberg atom count, the density of the Rydberg atoms within the guide, the velocity of the Rydberg atoms in the guide, and the fraction of remaining Rydberg atoms within the guide as a function of time.

We begin our detailed analysis with an explanation of the image magnifications. The ion distributions have a transverse magnification of $M_x = -1.6$, where the negative sign indicates inversion in the x direction due to an intermediate focal spot in the ion imaging [24]. This magnification is determined by moving the excitation beam by a known amount and measuring the resultant displacement in the image. The ion images have a longitudinal magnification of $M_z = 1$. Because the atoms travel in the guide with a constant average velocity, longitudinal position in the images is linked with time.

We detect an initial number of ∼30 ions per experimental cycle by integrating over the microwave ionization signal for $t_d = 5$ μs (immediate detection). Factoring in the detection efficiency of 15% and estimating that the excitation volume is a cylindrical region of 50-μm radius and 100-μm height, the actual number of Rydberg atoms initially present is ∼200 per experimental cycle and the corresponding density is of order 2×10^8 cm^{-3}. This is such a low density that Coulomb repulsion of the extracted ions is neither expected nor observed. Though this density is fairly low, it is sufficient to cause a fraction of the atoms to Penning ionize immediately following excitation and to l mix due to Rydberg-atom collisions. The Penning signal peaks at about 10 μs and becomes irrelevant after about 200 μs. We note that this time range is considerably longer than the Penning ionization time range observed in other work [25]. We attribute this difference to the fact that the atom guide allows the magnetically trapped atoms to maintain a relatively high chance of Penning ionization out to ∼100 μs.

Rydberg atoms that are initially excited into high magnetic field seeking states, or atoms that transition into such states, are expelled from the magnetic guide. A fraction of these atoms enter the strong electric field region due to the guard tube, where they are remotely field ionized. The resultant remote field ionization signal peaks at about 700 μs, as shown in Fig. 2(a). In the images, this remote field ionization signal is widely dispersed and spatially overlaps with the Rydberg-atom signal [Fig. 2(b)]. To eliminate the majority of the remote field ionization signal in the images, we gate the camera to selectively capture the microwave ionization component. In the gate timing, it is important to factor in the ion times of flight and the fluorescence decay of the phosphor screen. Our ion times of flight range from 3 to 25 μs, peaking at 10 μs. These long ion times of flight reflect the small electric fields present in the atom guiding region. The fluorescence lifetime of the phosphor screen is ≈50 μs, according to manufacturer specifications. We set the gate to range from just before the beginning of the microwave pulse to 150 μs beyond its end.

In Fig. 2 we compare an ungated [Fig. 2(b)] and a gated [Fig. 2(c)] image, both taken at a microwave ionization delay time of $t_d = 1.5$ ms. The dominant feature on the far left in the ungated picture is due to Penning ionization. We estimate that about ∼10% of detected ions are in this Penning ionization signal. This number varies with fluctuations in Rydberg atom density. Since each Penning collision involves a detectable ion as well as a second atom that transitions to a lower n state, about ∼20% of all Rydberg atoms created are involved in Penning ionization. Many counts from remote field ionization are also visible in the ungated images. The profiles in Fig. 2(d), taken by integrating Figs. 2(b) and 2(c) over the regions indicated by

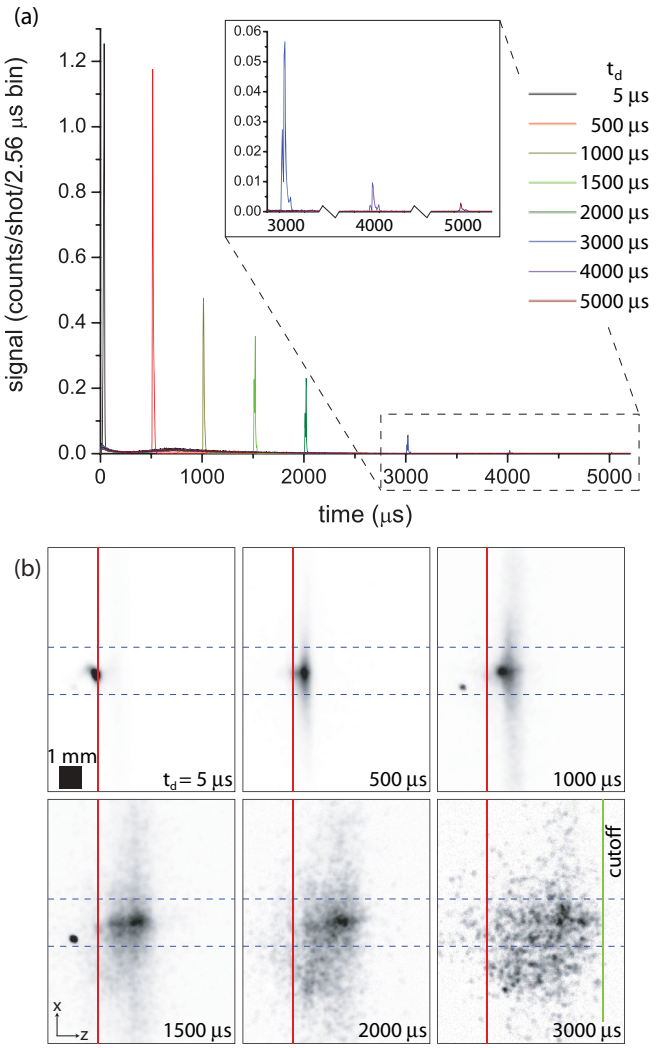

FIG. 3. (Color online) (a) MS traces as a function of delay time t_d. (b) Gated MCP images as a function of t_d. The brightness scale of each picture is optimized separately for clarity.

the dashed boxes, show that the gating removes about 17% of the signal near the microwave ionization peak and more than 50% in the wings. Therefore, in the ungated image the signal in the peak is mostly due to microwave ionization, whereas a large fraction of the signal in the wings is from the remote field ionization signal explained in the preceding paragraph. The benefit of the camera gating procedure primarily is to remove remote field ionization signal. The Penning ionization signal is also removed from the images, though this signal does not spatially overlap with the microwave ionization signal.

We study the evolution of the Rydberg atoms in the guide by varying the delay time t_d. Figure 3(a) shows MS traces for different values of t_d ranging from 5 μs to 5 ms. Figure 3(b) shows a selection of gated images. We have verified that all the signal in the images disappears when the microwave is turned off. The integrated microwave ionization signal in the MS traces in Fig. 3(a) corresponds to the signal seen in the images and gives a quantitative measure for the number of Rydberg atoms present in the guide at time t_d.

Based on the field gradient in the guide, we estimate that it takes a high magnetic field seeking Rydberg atom about 1 ms

to become expelled from the guide. This estimate is confirmed in the simulations described below. Hence the Rydberg-atom signal observed after ∼1 ms is primarily attributed to guided Rydberg atoms. As shown in the inset in Fig. 3(a), there is still microwave ionization signal at $t_d = 5$ ms, indicating that there is guiding of Rydberg atoms out to at least that time. For $t_d \geqslant 3$ ms the image is partially clipped by the edge of a slit in the electrode noted in Fig. 1, leading to a sharp cutoff in the ion images on the $+z$ side [see $t_d = 3$ ms in Fig. 3(b)]. The signal is only slightly cut off at $t_d = 3$ ms, but we miss detection of a significant amount of the signal at $t_d = 4$ ms and most of it at $t_d = 5$ ms.

The red lines in Fig. 3(b) mark the z location of immediate detection as a reference. The delayed guided-Rydberg-atom signals in Fig. 3(b) travel at an average speed of 1.2 m/s, indicating that the average forward speed of those atoms does not change upon excitation to Rydberg states. The velocity spread, given by the longitudinal extension of the ion signal divided by t_d, remains constant, which implies that Rydberg-atom collisions do not increase the longitudinal temperature of the atomic sample beyond its initial value of ∼1 mK.

The dashed lines in Fig. 3(b) represent the image location of the inner edges of the guide wires in the MCP plane (based on surface to surface wire separation of 1.5 mm and the measured magnification). The guide wires are a physical boundary on which Rydberg atoms become destroyed on impact. Thus, any atom detected outside the bounding lines must have come from the region above the guiding channel. These widespread counts arise at quite long delay times. A likely scenario that would explain the signal outside the horizontal bounding lines is that some atoms are guided for a significant amount of time before transitioning into high field seeking states, at which time they would be expelled from the guiding channel. The microwave pulse would ionize some of these atoms before they have traveled too far from the guiding region to be detected.

Profiles of the images in Fig. 3(b) in the x direction show that the Rydberg-atom distribution transverse to the guiding channel maintains an approximately constant shape up to $t_d =$ 1.5 ms. At later delay times, the fraction of the signal outside the dashed lines in Fig. 3(b) increases. This may indicate that at these later times an increasing fraction of unguided atoms contributes to the microwave ionization signal. However, at all delay times we observe a dense core in the images that is due to guided Rydberg atoms in low magnetic field seeking states.

Figure 4 shows the fraction of microwave-ionized Rydberg atoms as a function of t_d, with the experimental data plotted as squares. The data consistently give a signal decay time of $\tau_{\text{expt}} = 700 \pm 150$ μs, excluding the data points at $t_d = 4$ and 5 ms, where much of the signal is blocked by the edge of the slit. The value of τ_{expt} is significantly longer than the natural decay time of the $59D_{5/2}$ state, $\tau_{59D5/2} = 150$ μs, indicating a collision-induced, near-instantaneous increase in lifetime following excitation.

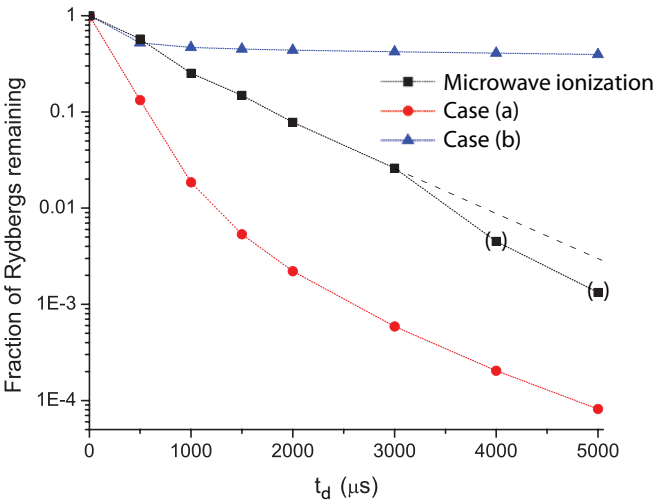

FIG. 4. (Color online) Fraction of Rydberg atoms remaining vs delay time t_d from experiment (squares) and simulation with l mixing (triangles) and without l mixing (circles). The parentheses indicate points where a significant portion of the experimental signal is blocked from detection. The dashed line shows an extrapolation of the experimental curve based on the assumption that the Rydberg signal decay time does not change after 4 ms, where the signal is partially blocked.

IV. NUMERICAL SIMULATIONS

We compare the experimental data to a simulation in which the center-of-mass dynamics of the atoms are treated classically while the internal-state evolution is treated by simulating the transitions of the Rydberg atoms between internal states via discrete quantum jumps. At each time step of the simulation, each Rydberg atom is in a well-defined state $|n,l,j,m_j\rangle$, with the quantization axis given by the direction of the magnetic field at the atom's location. Since the center-of-mass dynamics are several of orders of magnitude slower than the internal dynamics, we may assume that the internal states of the atoms adiabatically follow the changes in magnetic field direction. Since a magnetic field B_0 of several gauss is applied along the wire direction, the magnetic field anywhere in the guide is larger than B_0 and nonadiabatic transitions from trapped to untrapped states do not occur. Also, the m_j values and Landé g factors of the atoms are well defined at all times, allowing for straightforward integration of the center-of-mass dynamics in the magnetic guiding field. To simulate internal-state quantum jumps we have numerically calculated the spontaneous transition rates, thermally induced transition rates, and photoionization rates for all electric dipole transitions between Rydberg and unbound states at 300 K. All transition rates less than 1 s^{-1} are neglected since we simulate the evolution over a time interval of only 5 ms. A time step size of 5 μs is used. This is sufficiently short to accurately model the center-of-mass motion because it is orders of magnitude less than the center-of-mass oscillation period of the atoms in the guide. It is also sufficiently short to model the radiative transitions between the internal atomic states because the shortest transition times for the states of interest are longer than ∼100 μs. At each time step of the calculation the transition probabilities for the allowed transitions and for photoionization are calculated (for the chosen time step size the transition probabilities add up to a number much less than 1). In each time step and for each atom a new random number is used to determine whether the atom remains in its current state, photoionizes, or undergoes a transition into a different Rydberg state. If the last decay branch is selected, an additional

random number is used to determine the target state. Also, if the atom undergoes a transition into a different Rydberg level the magnetic moment is updated according to the m quantum number and the g factor of the new state. The model accounts for guided-atom loss due to thermal photoionization, decay toward the ground state, lifetime increases of the guided-atom population due to thermal transitions into states with higher n and l, and radiatively-driven probability flow between the guided domain ($m_j > 0$) and the unguided domain ($m_j \leqslant 0$). The simulation does not account for Rydberg atom collisions with other particles.

Although the Rydberg atom samples we prepare in the experiment are not very dense, we do observe Penning ionization at early times, which suggests some degree of initial state mixing of the remaining non-Penning-ionized atoms. After the Penning ionization ceases, we expect collision-free evolution. The simulations are therefore run for two types of initial conditions. In case (a), the atoms are initially prepared in the $59D_{5/2}$ level with randomly selected m_j values. Here, we model a collision-free situation in which the atoms evolve independently, solely due to radiative transitions between internal states and the magnetic force acting on the center-of-mass coordinates. In case (b), the atoms are initially prepared with an effective quantum number $n^* \approx 58$ and (l, j, m_j) quantum numbers randomly selected in a manner that the probabilities of all possible quantum states are identical (namely, $1/2n^{*2}$). Here, we simulate the effects of an initial phase of complete l and m mixing due to Rydberg-atom collisions, which randomize all angular quantum numbers of the Rydberg atoms to result in a shell averaged sample.

In Fig. 4 we compare the experimentally observed fraction of remaining Rydberg atoms as a function of t_d with the simulation [case (a), circles; case (b), triangles]. In simulation case (a), over the first 2 ms the signal decay time gradually increases from about 200 μs to 1 ms due to thermal transitions. In contrast, in the experiment the transition into longer-lived Rydberg levels occurs on a near-instantaneous time scale. The decay behavior of the experimental data and simulation case (a) match fairly well at $t_d \gtrsim 2$ ms; however, the experimental data consistently exceed the simulated ones by a factor of $\sim$50 in that time domain. We attribute this difference in behavior to the aforementioned Penning-ionizing collisions, which apparently cause a rapid, near-instantaneous state mixing and an associated fivefold increase of the signal decay time. The signal decay time in the simulation case (b), $\tau_b = 33 \pm 5$ ms, is about 30 times longer than the experimental value, indicating that the collision-induced l mixing in the experiment falls far short of producing a shell-averaged sample. We conclude that the experimental results lie between simulation cases (a), with no initial collision-induced mixing, and (b), with complete initial collision-induced l and m mixing. In particular, initial collisions do not populate any extremely long-lived high-l states.

V. CONCLUSION

We have observed guiding of Rydberg atoms in a high-gradient linear magnetic guide for up to 5 ms. To detect the atoms, we utilized a microwave ionization technique. We found a guided Rydberg atom signal decay time nearly five times longer than the lifetime of the initial $59D_{5/2}$ state. In view of simulations, the increase in decay time is due to initial l-mixing collisions and thermal transitions. The physical setup of our experiment limits the detection region such that we are only able to detect guiding of the Rydberg atoms over about 1 cm. In the future, one may realize much longer Rydberg atom guiding times (and therefore guiding distances) by exciting long-lived circular-state Rydberg atoms in the guide using adiabatic state-preparation techniques [26], which are compatible with our experimental apparatus.

ACKNOWLEDGMENTS

This work has been supported by the Army Research Office (Grant No. 50396-PH). M.T. acknowledges support by a National Defense Science & Engineering Graduate fellowship.

[1] O. Mülken, A. Blumen, T. Amthor, C. Giese, M. Reetz-Lamour, and M. Weidemüller, Phys. Rev. Lett. **99**, 090601 (2007).
[2] M. Müller, L. Liang, I. Lesanovsky, and P. Zoller, New J. Phys. **10**, 093009 (2008).
[3] H. Weimer, R. Löw, T. Pfau, and H. P. Büchler, Phys. Rev. Lett. **101**, 250601 (2008).
[4] T. Pohl, E. Demler, and M. D. Lukin, Phys. Rev. Lett. **104**, 043002 (2010).
[5] M. D. Lukin, M. Fleischhauer, R. Cote, L. M. Duan, D. Jaksch, J. I. Cirac, and P. Zoller, Phys. Rev. Lett. **87**, 037901 (2001).
[6] M. Saffman, T. D. Walker, and K. Mølmer, Rev. Mod. Phys. **82**, 2313 (2010).
[7] J.-H. Choi, J. R. Guest, A. P. Povilus, E. Hansis, and G. Raithel, Phys. Rev. Lett. **95**, 243001 (2005).
[8] S. D. Hogan and F. Merkt, Phys. Rev. Lett. **100**, 043001 (2008).
[9] S. E. Anderson, K. C. Younge, and G. Raithel, Phys. Rev. Lett. **107**, 263001 (2011).
[10] I. Lesanovsky, J. Schmiedmayer, and P. Schmelcher, Phys. Rev. A **70**, 043409 (2004).
[11] I. Lesanovsky, J. Schmiedmayer, and P. Schmelcher, Europhys. Lett. **65**, 478 (2004).
[12] I. Lesanovsky and P. Schmelcher, Phys. Rev. Lett. **95**, 053001 (2005).
[13] B. Hezel, I. Lesanovsky, and P. Schmelcher, Phys. Rev. Lett. **97**, 223001 (2006).
[14] U. Schmidt, I. Lesanovsky, and P. Schmelcher, J. Phys. B **40**, 1003 (2007).
[15] M. Mayle, I. Lesanovsky, and P. Schmelcher, Phys. Rev. A **80**, 053410 (2009).
[16] M. Mayle, B. Hezel, I. Lesanovsky, and P. Schmelcher, Phys. Rev. Lett. **99**, 113004 (2007).
[17] N. H. Dekker, C. S. Lee, V. Lorent, J. H. Thywissen, S. P. Smith, M. Drndić, R. M. Westervelt, and M. Prentiss, Phys. Rev. Lett. **84**, 1124 (2000).

[18] P. D. D. Schwindt, E. A. Cornell, T. Kishimoto, Y.-J. Wang, and D. Z. Anderson, Phys. Rev. A **72**, 023612 (2005).
[19] M. Ke, X.-L. Li, and Y.-Z. Wang, Chin. Phys. Lett. **25**, 907 (2008).
[20] S. D. Hogan, J. A. Agner, F. Merkt, T. Thiele, S. Filipp, and A. Wallraff, Phys. Rev. Lett. **108**, 063004 (2012).
[21] S. E. Olson, R. R. Mhaskar, and G. Raithel, Phys. Rev. A **73**, 033622 (2006).
[22] R. R. Mhaskar, S. E. Olson, and G. Raithel, Eur. Phys. J. D **41**, 221 (2007).
[23] J. L. Wiza, Nucl. Instrum. Methods **162**, 587 (1979).
[24] V. D. Vaidya, M. Traxler, C. Hempel, R. R. Mhaskar, and G. Raithel, Rev. Sci. Instrum. **81**, 043109 (2010).
[25] P. J. Tanner, J. Han, E. S. Shuman, and T. F. Gallagher, Phys. Rev. Lett. **100**, 043002 (2008).
[26] A. Nussenzweig, J. Hare, A. M. Steinberg, L. Moi, M. Gross, and S. Haroche, Europhys. Lett. **14**, 755 (1991).